AD-A129 785 STIMULATED BRILLOUIN BACKSCATTER IN LONG SCALE LENGTH 1/1
PLASMAS(U) NAVAL RESEARCH LAB WASHINGTON DC
D G COLOMBANT ET AL. 24 JUN 83 NRL-MR-5118

UNCLASSIFIED F/G 20/9 NL

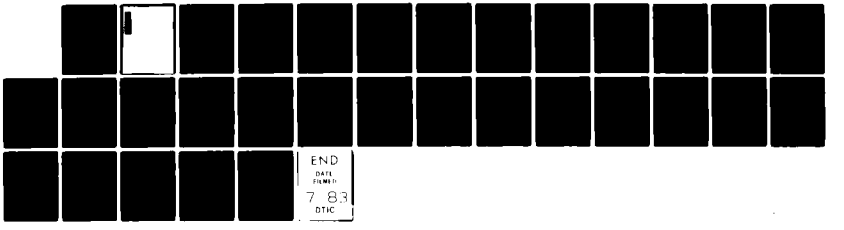

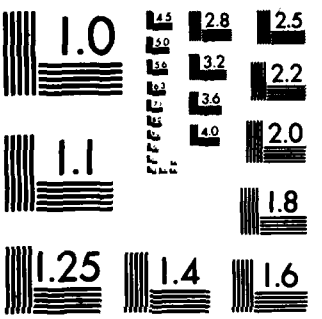

SECURITY CLASSIFICATION OF THIS PAGE (When Data Entered)

REPORT DOCUMENTATION PAGE		READ INSTRUCTIONS BEFORE COMPLETING FORM
1. REPORT NUMBER NRL Memorandum Report 5118	2. GOVT ACCESSION NO. AD-A124785	3. RECIPIENT'S CATALOG NUMBER
4. TITLE (and Subtitle) STIMULATED BRILLOUIN BACKSCATTER IN LONG SCALE LENGTH PLASMAS		5. TYPE OF REPORT & PERIOD COVERED Interim report on a continuing NRL problem. 6. PERFORMING ORG. REPORT NUMBER
7. AUTHOR(s) D.G. Colombant, W.M. Manheimer and J.H. Gardner		8. CONTRACT OR GRANT NUMBER(s)
9. PERFORMING ORGANIZATION NAME AND ADDRESS Naval Research Laboratory Washington, DC 20375		10. PROGRAM ELEMENT, PROJECT, TASK AREA & WORK UNIT NUMBERS DE-AI08-79DP40092; 47-0859-0-3
11. CONTROLLING OFFICE NAME AND ADDRESS U.S. Department of Energy Washington, DC 20545		12. REPORT DATE June 24, 1983 13. NUMBER OF PAGES 30
14. MONITORING AGENCY NAME & ADDRESS(if different from Controlling Office)		15. SECURITY CLASS. (of this report) UNCLASSIFIED 15a. DECLASSIFICATION/DOWNGRADING SCHEDULE

16. DISTRIBUTION STATEMENT (of this Report)

Approved for public release; distribution unlimited.

17. DISTRIBUTION STATEMENT (of the abstract entered in Block 20, if different from Report)

18. SUPPLEMENTARY NOTES

This work was supported by the U.S. Department of Energy.

19. KEY WORDS (Continue on reverse side if necessary and identify by block number)

Stimulated Brillouin backscatter
Laser fusion plasmas
Instabilities

20. ABSTRACT (Continue on reverse side if necessary and identify by block number)

Stimulated Brillouin backscatter in long scale length plasmas is calculated using a wave kinetic model. These calculations make use of computer hydrodynamic profiles for these plasmas. Results are presented for the parameters of the joint NRL - LLNL experiments and for reactor size pellets of 5 mm characteristic length. Means of reducing high levels of backscatter for the latter case are investigated.

DD FORM 1 JAN 73 1473 EDITION OF 1 NOV 65 IS OBSOLETE
S/N 0102-014-6601

SECURITY CLASSIFICATION OF THIS PAGE (When Data Entered)

CONTENTS

STIMULATED BRILLOUIN BACKSCATTER IN LONG SCALE LENGTH PLASMAS

I. Introduction

This paper studies stimulated Brillouin backscatter in long scale length and reactor scale length laser produced plasmas.

Previous experiments on laser ablative acceleration on short scale length plasmas show that in the regime around 10^{13} W/cm^2 for 1 μ light, stimulated Brillouin backscatter is not a serious problem.[1-3] A first indication of the potential importance of stimulated scatter on long scale length plasmas has recently been obtained from a joint NRL - LLNL experiment on SHIVA in which nearly millimeter scale length plasmas were produced by a Nd laser at about 10^{14} W/cm^2.[4] There it was found that scattered light is about 50% of the incident light. Since ray tracing codes generally predict better than 90% absorption, it is clear that some anomalous scattering process is taking place.

In this work, we model this scattering as stimulated Brillouin backscatter. Although the frequency of the scattered light is consistent with this, the angular distribution of the scattered light is nearly uniform over 2π solid angle. Thus, our basic assumption is that one can average over backscattering direction and then model the process as all occurring in a single direction, in our case direct backscatter. In a future work we will examine the angular dependence of the backscatter.

To model the backscatter, we use a scheme which we have derived previously[5] for integrating the incident and reflected intensities through the spatially varying underdense plasma. A similar scheme has been proposed recently by others.[6] Although this scheme does not provide the sort of detailed knowledge of the microphysics available in a particle simulation, it is clear that running a particle simulation for the length scales involved ($L_n \sim$ 1mm, $\lambda \sim 1\mu$m) would be prohibitively expensive. Also, particle

Manuscript approved April 27, 1983.

simulations are best in demonstrating the different nonlinear effects on the sound wave itself (i.e. harmonic generation, wave breaking, trapping, etc). However, as we shall see, for the millimeter scale length plasmas we consider, there are almost certainly no nonlinear effects on the sound wave.

In the next section, we describe the basic theory and formalism. In Section III, we apply this to calculating backscatter for the NRL - LLNL joint experiment and also to reactor scale plasmas. In all cases, we find that the presence of a velocity gradient is an extremely important stabilizing effect. Generally, we find that for irradiances of $I \approx 10^{14} W/cm^2$, stimulated backscatter can be held to tolerable levels for 5 mm pellets, but not at $I \approx 3 \times 10^{14}$ W/cm^2. For these latter pellets, we examine the effect of three processes which might reduce the backscatter; greater dissipation, shorter laser wavelength and use of a broadband laser. This last process has by far the largest stabilizing effect if the bandwidth can be made of order 1%.

II. Theory

The basic equations which we use to describe the Brillouin backscatter process are as described in Ref. 5. They are

$$V_p \frac{d}{dx} |A_p|^2 + 2|A_p|^2 \frac{dV_p}{dx} + 2\nu_p |A_p|^2 = - V_r \frac{d}{dx} |A_r|^2$$

$$- 2|A_r|^2 \frac{dV_r}{dx} - 2\nu_r |A_r|^2 = - \frac{2\gamma_o^2 |A_p|^2 |A_r|^2 \nu_s / V_s^2}{(k_p - k_r - k_s)^2 + (\nu_s / V_s)^2} . \qquad (1)$$

where the sound wave is assumed to be in the strong damping regime. In Eq. (1), the subscripts p,r, and s denote the pump (laser), reflected wave, and sound wave respectively. The quantity A^2 denotes the action density, $A^2 = \partial\varepsilon/\partial\omega \; E^2$ where E is the electric field amplitude of the wave. Other quantities regarding the electromagnetic waves are the wave vectors,

$$k_p = c^{-1}(\Omega_p^2 - \omega_{pe}^2)^{1/2} \qquad (a)$$

$$k_r = - c^{-1}(\Omega_r^2 - \omega_{pe}^2)^{1/2} \qquad (b) \qquad (2)$$

where $\Omega_{p,r}$ is the frequency of the pump or reflected wave; the group velocities

$$V_p = \frac{k_p c^2}{\Omega_p} \qquad (a)$$

$$V_r = \frac{k_r c^2}{\Omega_r} \qquad (b) \qquad (3)$$

and inverse bremsstrahlung damping rate

$$\nu_r = \nu_p = \frac{1}{2} \frac{\omega_{pe}^2}{\Omega^2} n_p Z \ln \Lambda / 3.5 \times 10^5 T_e^{3/2}(eV). \qquad (4)$$

The coupling coefficient γ_o is given by

$$\gamma_o = \frac{\omega_{pi}}{m\Omega_p} \frac{e(M/Zm)^{1/4}}{(cV_e)^{1/2}} \left(\frac{2\pi\Omega_p}{1 + k_p^2 c^2/\Omega_p^2}\right)^{1/2}. \qquad (5)$$

Equation (1) is written for planar geometry. For spherical geometry, we simply make the replacement $\frac{d}{dx} \rightarrow \frac{1}{r^2} \frac{d}{dr} r^2$. To account for either a broadband pump, or a wide spectrum of reflected waves, we simply replace the right hand side of Eq. (1) with the appropriate summation over incident or reflected waves. In this paper, we will present calculations for a broadband pump with a single reflected wave, and calculations for a single frequency pump with a wide spectrum of scattered waves. We compare the case of wide band reflection with the case of a single reflected wave where the resonant position varies. It turns out that the total scattered light for a wide band noise source is, as expected, approximately equal to an average over different resonant positions.

For the case of a single incident and single reflected wave, the laser irradiance is specified at $x = -\infty$ (zero density) and the reflected wave is specified at the critical density. If there is more than one reflected wave, or more than one incident frequency in the pump, then the total reflected or incident power is divided up among the different frequency components so that the sum is as specified. For the case of several different frequency pump waves and one reflected wave, the incident spectrum is specified at $x = -\infty$ and the calculation is iterated until the reflected wave has the proper irradiance at the critical density. For the case of a single frequency pump and several reflected waves, the reflected spectrum is specified at the

critical density and the calculation is iterated until the incident wave has the proper irradiance at $x = -\infty$. The case of a spectrum of both incident and reflected waves would clearly involve a multidimensional iteration and has not been attempted.

Let us consider the case of a single reflected wave and a broadband pump, and compare it with broadband reflected light and a broadband pump. For the case of a single reflected wave, the reflected wave starts at critical density, propagates through the underdense plasma, and at various positions, resonates with one of the waves in the pump and amplifies. Now imagine that reflected wave is split into two frequency components, each one having half the irradiance at the critical density. Assume further that each wave is resonant at the same position. (For instance, the incident pump might consist of six equal irradiance waves, of which only four can resonate with one of the reflected waves. The other reflected wave might resonate with a different set of four waves, but at the same positions in the plasma.) Then, each reflected wave is amplified the same amount while in the linear regime. Since each wave has half the amplitude, but there are twice as many of them, the total amplification is the same. This shows that for a broadband pump, any difference between single and broadband reflected light arises from nonlinearities and spectral shape (as opposed to total integrated spectrum). We do not expect these differences to be significant, and this expectation is largely confirmed by our studies of broadband, compared to single wave reflected light for a single wave pump.

Since the sound wave is assumed to be in strong damping limit, all phase information drops out of Eq. (1) and the sound wave amplitude is given by

$$|A_s^2| = \frac{(\gamma_o^2/V_s^2)|A_p^2||A_r^2|}{(k_p - k_r - k_s)^2 + (\nu_s/V_s)^2} \qquad (6)$$

where the sound wave group velocity and wave number are given by

$$V_s = V + C_s \qquad (a)$$

$$k_s = \frac{\Omega_p - \Omega_r}{V_s} \qquad (b). \qquad (7)$$

Here C_s is the sound speed, assumed positive, and V is the flow velocity. For our assumed configuration with k_p positive and k_r negative, V is negative. Thus blue shifted reflected light ($\Omega_r > \Omega_p$) implies supersonic flow. For all cases we study, the flow turns out to be supersonic. The one remaining quantity to specify is the sound wave damping rate ν_s. Rather than relate this to plasma parameters, we assume phenomenological values which vary between $|\Omega_r - \Omega_p|/40 < \nu_s < |\Omega_r - \Omega_p|/5$. As we shall see, the stimulated backscatter is quite insensitive to this parameter, as discussed in Ref 5.

Notice that the only nonlinear effect included in Eq. (1) is pump depletion. As we have shown in our previous work,[5] this assumption is valid in long scale length plasmas where $e\phi_s/T_e$ remains small even though the backscatter may be large. Calculations of $e\phi/T_e$, in the long scale length plasma studied here, show that it is everywhere less than about three percent, so nonlinear effects on ion sound wave would not be expected to be very important.

The procedure then is to pick density, velocity, and temperature profiles from numerical simulations of the fluid motion of a long scale length laser produced plasma. Using these profiles, Eqs. (1) are solved numerically assuming an incident pump wave of given irradiance at low density, and a thermal noise source for the reflected wave at the critical density. The final result does depend on the thermal noise source, but once the reflection

enters a regime where pump depletion plays a role, this dependence becomes very much weaker than what one might expect. For instance, we will show that varying the thermal noise source by four orders of magnitude can change the reflection coefficient by as little as ten percent. We find that a thermal noise source of 10^{-4} times the incident irradiance gives best agreement with the joint experiment.

III. Results

Results are presented for several types of laser produced plasmas. First, in an attempt to evaluate the model, Brillouin backscatter was calculated for plasma conditions corresponding to the joint Naval Research Laboratory - Lawrence Livermore National Laboratory experiments.[4] These experiments were carried out on Shiva in order to check scaling of non-uniformities with laser irradiance. Back and side scatter were also measured as part of the experiments since the plasmas produced involved long scale lengths. Since concern for backscatter increases with the scale length of the plasma, calculations have also been performed for 5 mm reactor size pellets. High levels of backscatter are found in this case when the irradiance reaches several times 10^{14} W/cm^2. Means of reducing backscatter are then considered: increased dissipation, shorter wavelength laser light and broadband pump.

1. Joint NRL - LLNL experiment.

These experiments were performed on CH planar targets with 1 μm laser light at irradiances comprised between 1 and 2 x 10^{14} W/cm^2. Simulations of these experiments were made using a 1D code developed at NRL.[7] Flow profiles in the underdense plasma are shown in Fig. 1 at t=3 nsec for characteristic parameters of these experiments. A 25 μm CH foil is irradiated with a 1 μm laser light pulse, ramping up linearly in 2.6 nsec and remaining constant for an additional 0.4 nsec. The irradiance quoted in Fig. 1 is the absorbed irradiance. Quasi steady-state was reached at t = 3 nsec and backscatter was computed using these profiles and is presented in Fig. 2. In all calculations except one which will be mentioned, the sound wave damping rate was taken equal to $|\Omega_r - \Omega_p|/10$. In Fig. 2 as well as in other figures, calculations for reflectivity are presented as a function of resonant density (normalized to

critical density) where the reflected wave resonates with the pump and the sound waves.

In calculating the backscatter, we first assume that a certain level of backscatter is tolerable in a laser fusion scheme (here we assume this is 33 1/3%). Then we assume an incident irradiance 50% greater than the absorbed irradiance used in the fluid simulation. If the calculated backscatter is 33 1/3%, our assumption is consistent. A calculation of more than 33 1/3% backscatter means the backscatter will be greater than this, and vice versa. For comparison, we also show the calculated backscatter assuming the incident irradiance is equal to the absorbed irradiance. Thus for the joint experiment, we show calculations of backscatter assuming both $I = 1.5 \times 10^{14}$ and 10^{14} W/cm^2. Thermal noise in the vicinity of the critical density has been assumed to be 10^{-4} smaller than the pump wave intensity. One point on the graph indicates the reflectivity for the 1.5×10^{14} W/cm^2 case for thermal noise 4 orders of magnitude smaller, i.e. 10^{-8} smaller than the pump intensity. From Fig. 2, we see that the maximum backscatter occurs for a resonant density approximately equal to 0.35 times the critical density and is about 45%. The average backscatter is about 35%. These results agree well with that found experimentally - 65% absorption[2,4] - except that the experiments indicate a significant amount of sidescatter. The reflection corresponding to the reduced thermal noise is only 27% for $n_{res} = 0.4\ n_{crit}$ which seems to indicate that this value of thermal noise is underestimated.

Before knowing the exact values of the irradiance in these joint experiments, tests had been made at lower intensities in order to check on results obtained previously. In Fig. 3, results of reflectivity are presented at $I = 4.1 \times 10^{13}$ W/cm^2 (with correspondingly different flow profiles) with and without velocity gradients for a thermal noise of 10^{-8}. More than 6

orders of magnitude separate the reflectivity for these two cases and it shows once again the importance of including velocity gradients in backscatter calculations. The influence of thermal noise amplitude was also investigated in a systematic way for irradiance of 7×10^{13} W/cm^2. We see in Fig. 4 that the backscatter is proportional to the noise when the backscatter is small ($\lesssim 10^{-2}$). However, as soon as the level of backscatter increases, non-linear effects (pump depletion is the only non-linear effect included in this model) become important and reduce the difference between the two cases. For the case in Fig. 2, where the backscatter is higher, the relative difference between the thermal noise levels is smaller still.

2. Reactor size pellets

The next calculation involves reactor size pellets. These calculations were made using the same code in spherical geometry. Laser light of $\pi \times 10^{14}$ Watts is absorbed by a pellet with initial radius of 5 mm. Because of the spherical geometry, it was assumed that the light was focussed at the center of the pellet. The same approximation was made in the hydrodynamical and Brillouin calculations. A flux limiter of 0.1 was used in the hydrodynamical calculations. Profiles for the flow characteristics are shown in Fig. 5 at t = 12 nsec into the run. The laser pulse shape is once again assumed to ramp up linearly in 2 nsec and then to remain constant afterwards. Results for reflectivity are shown in Fig. 6 as a function of resonant density for the reflected wave and for two incident wave irradiances (1.5×10^{14} and 10^{14} W/cm^2 respectively). The maximum reflection for this case occurs at $n_{res}/n_{crit} \approx 0.3$ and is about 20%. Thus, the refelectivity for this case is smaller than that shown previously for the joint NRL - LLNL experiments. The main reason for this apparently surprising result is that in spherical geometry, irradiance drops rapidly with radius. At 8 mm for

example, the irrandiance is only 40% of its nominal value at 5mm.

The irradiance was then raised to 3 times its previous value for the same pellet and the hydrodynamic proriles are shown in Fig. 7 while reflectivity is shown in Fig. 8. The gradients are smaller in this case and the backscatter reaches levels of 60% for $n_{res}/n_{crit} = 0.25$.

In calculations done up to this point, only one backscatter wave is included. To test the validity of this approximation, we have redone this calculation with 5 backscattered waves at five resonant densities (n/n_{crit} = 0.1 - 0.5) simultaneously included. The absorbed power was $3\pi \times 10^{14}$ Watts. The reflectivity as a function of irradiance is shown in Fig. 9. It is roughly equal to the maximum reflectivity obtained when the calculation included independent single backscattered waves. Notice also that the reflectivity at 10^{14} W/cm^2 is very similar to that found in Fig. 6 although the hydrodynamic profiles were calculated for 10^{14} W/cm^2 there. Also shown in Fig. 9 is the relative backscattered spectrum at different irradiances. We see that the dominant modes shift to lower resonant densities as the irradiance increases. Because of its weak dependence on absorbed irradiance, this curve can be used as a general guide for reflectivity vs. irradiance for 5 mm size pellets. Although it shows that laser-target coupling is satisfactory up to about 2×10^{14} W/cm^2, it raises questions about coupling above that irradiance. Because of the high levels of backscatter anticipated at these higher irradiances, ways of reducing SBS have been investigated. They are in the order of the presentation below, increased dissipation, shorter wavelength laser light and broadband pump.

3. Reduction in Brillouin Backscatter

   a) Increased dissipation rate

      In all the results presented so far, we have assumed $\nu_s/\omega_s = 0.1$

where ω_s is the frequency of the sound wave in the frame of the plasma flow. In Fig. 10, we show variations of the reflectivity for the 5 mm pellet case at $n_{res}/n_{crit} = 0.30$ for an incident irradiance of 3×10^{14} W/cm^2. The choice of the resonant density was made in order to avoid problems associated with the dimension of the interaction region. Figure 10 shows that the reflectivity remains approximately constant as the dissipation rate varies by an order of magnitude. It was pointed out in ref. 5 that as the damping of the sound wave increases, the region over which the instability occurs also increases and as a result, the reflectivity remains roughly constant.

Also shown in Fig. 10 is the maximum value for $e\phi/T_e$ reached in the calculation. We see that it reaches a maximum value of 1.5% for the lower dissipation rate down to 0.5% for the higher one. This maximum is usually located downstream of the resonant point. These values for $(e\phi/T_e)_{max}$ justify a posteriori the strong damping limit which has been used in the present model, and also the neglect of nonlinear effects on the sound wave.

b) Shorter wavelength laser light.

Shorter wavelength laser light presents several advantages for laser fusion[8] and it is important to see how it performs as far as Brillouin backscatter is concerned. Calculations for the 5 mm pellet were redone for 0.53 μm light and new profiles were calculated for 3×10^{14} W/cm^2 absorbed at t = 12 nsec. These are shown in Fig. 11. It can be seen on this figure that the density gradient scale length is shorter in the underdense plasma for the 0.53 μm case and that the velocity gradient scale length is about the same. The backscatter results are shown in Fig. 12 and show that the average reflectivity has been reduced from about 60% for the 1 μm light to about 12% for 0.53 μm light. The reduction in backscatter results from both increased collisional absorption and also the smaller value of electron oscillating

velocity compared to thermal velocity. Although it is quite satisfactory, it is interesting to investigate other ways of reducing Brillouin backscatter.

c) Broad bandpump

For these calculations, it has been assumed that the pump was made up of 9 modes with a spread in frequency between the outmost wing and the center frequency denoted by $\Delta\Omega$. The pump spectrum is assumed to be uniform and only one reflected wave resonant with the center pump mode at $n_{res}/n_{crit} = 0.3$ - near the maximum of the reflection curve - was kept in the calculation. Results were obtained for 1 μm laser light for the 5 mm radius pellet case for an incident irradiance of $4.5 \times 10^{14} W/cm^2$. Results of reflection as a function of $\Delta\Omega/\Omega$ appear in Fig. 13. A dramatic decrease in reflection is achieved for $\Delta\Omega/\Omega \approx 1\%$ since the reflection has dropped to about 10%. This result seems to be the most encouraging result so far in our backscatter studies. Even for schemes for laser fusion where long wavelength has been suggested to illuminate the pellet, it offers the possibility of reducing the backscatter at acceptable levels and thus of achieving satisfactory coupling between the incident laser light and the target.

Conclusion

In summary, we have presented calculations of Stimulated Brillouin Backscatter for long scale length plasmas. First, for the case of the joint NRL-LLNL experiment (λ = 1.06 μm, $I_{abs} \approx 10^{14}$ W/cm^2), we have seen that our calculations reproduce the experimental value for the total reflection if the background noise for the reflected wave is taken 4 orders of magnitude below the pump wave in the vicinity of the critical density. A characteristic of the experiment which is not accessible to our model, is the flat angular distribution of the reflected signals.

For the reactor size pellets, the 5 mm case at $I_{abs} = 10^{14}$ W/cm^2 present low levels of backscatter because of the lower irradiance at larger radii. The same case for $I_{abs} = 3 \times 10^{14}$ W/cm^2 presents much higher levels of backscatter (up to 60%) and raises serious doubts about coupling of laser light to the target for that case. Several means of reducing those high levels have been investigated. Besides the gain achieved in shortening the laser light incident wavelength, the most effective way of reducing the backscatter to almost insignificant levels (less than 10%) is to use a broadband pump with frequency spread $\Delta\Omega/\Omega$ of the order of 1%.

Acknowledgments

The authors would like to thank Dr. S. Bodner for his support in this study. This work was supported by the U. S. Department of Energy.

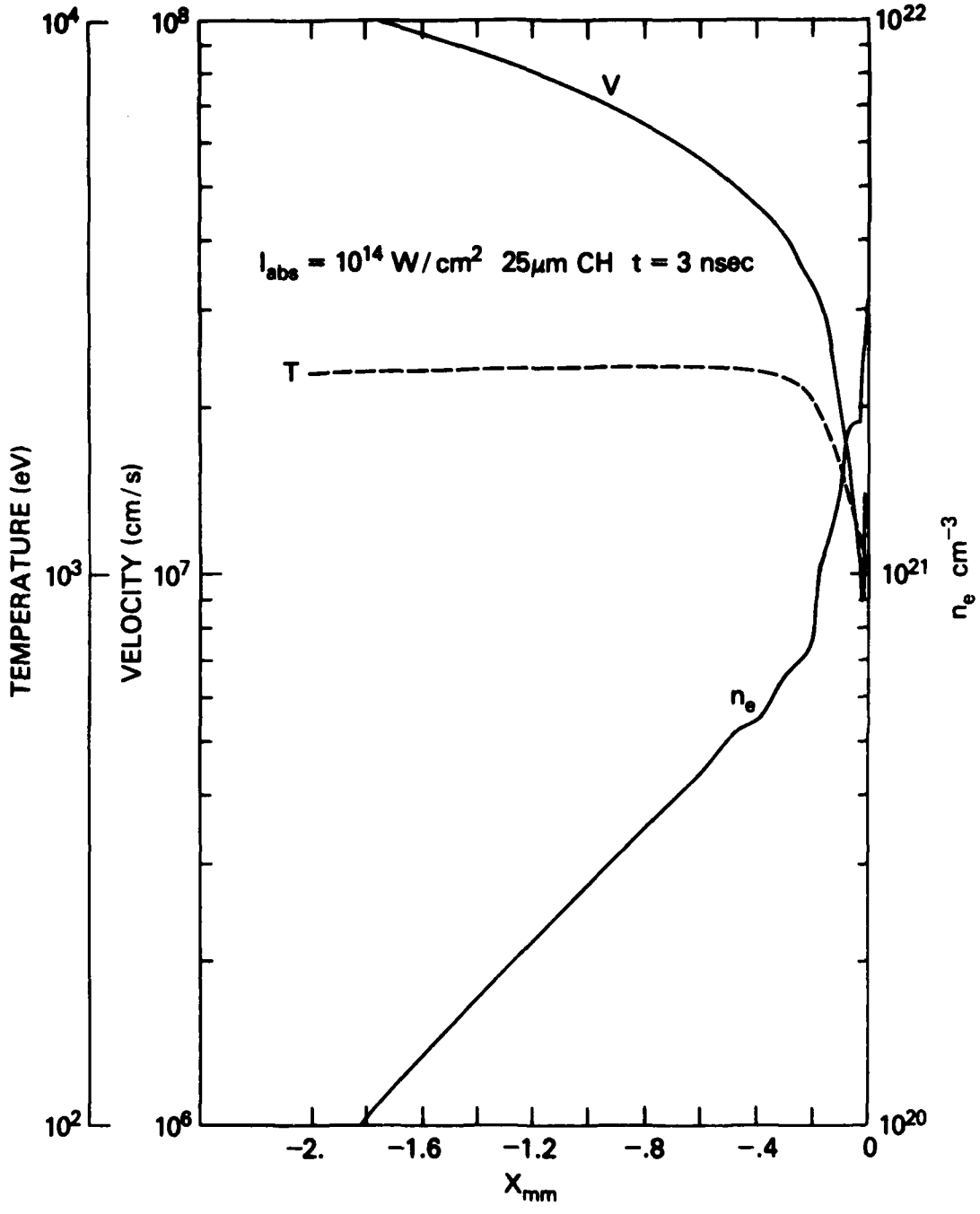

Fig. 1. Flow profiles used in Brillouin calculations for 10^{14} W/cm^2, 1 μ laser light impinging on 25 μm CH planar target after steady-state conditions have been reached (t = 3 nsec). Note that laser irradiance refers to absorbed irradiance, not incident.

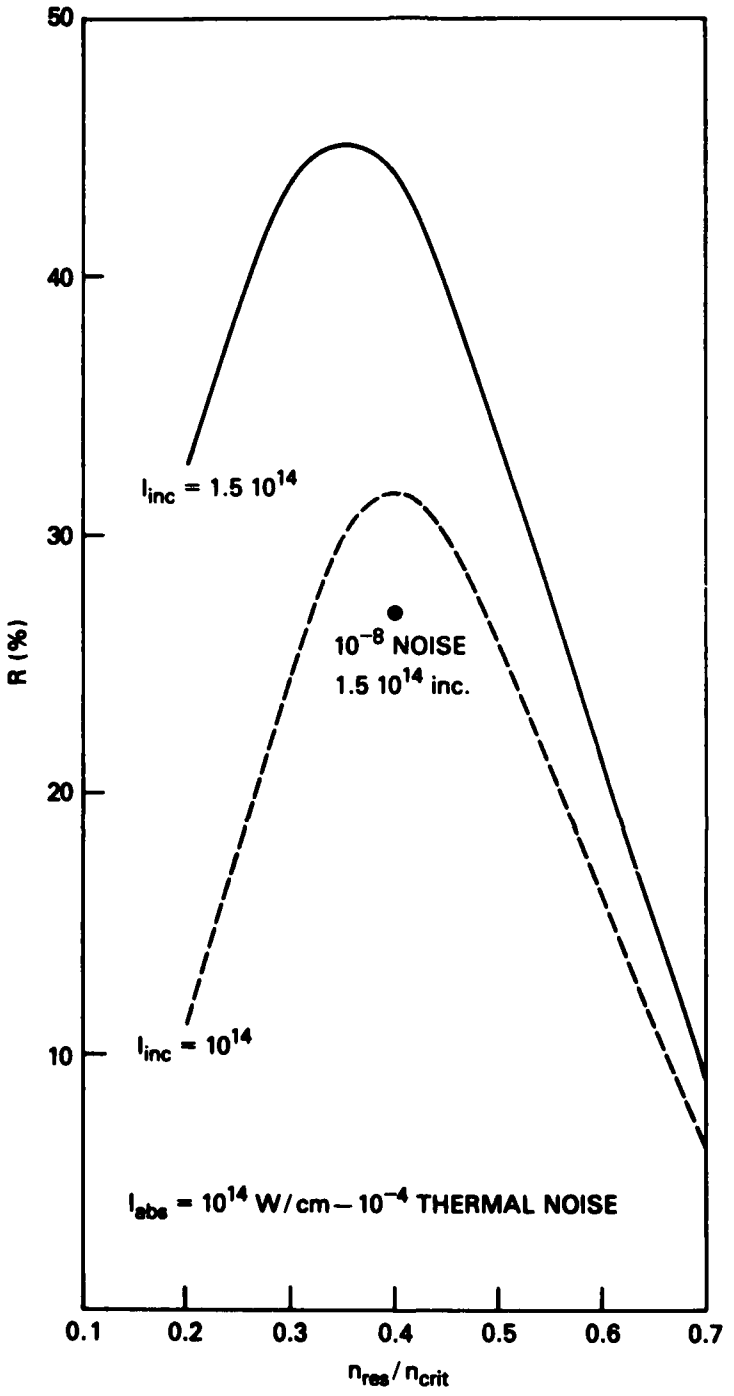

Fig. 2 Reflectivity for the case of Fig. 1 as a function of the resonant density of the reflected wave. Curves are shown for incident irradiance of 1.5 10^{14} W/cm^2 and 10^{14} W/cm^2. Also, one point on the graph has been calculated for thermal noise 8 orders of magnitude below the pump intensity.

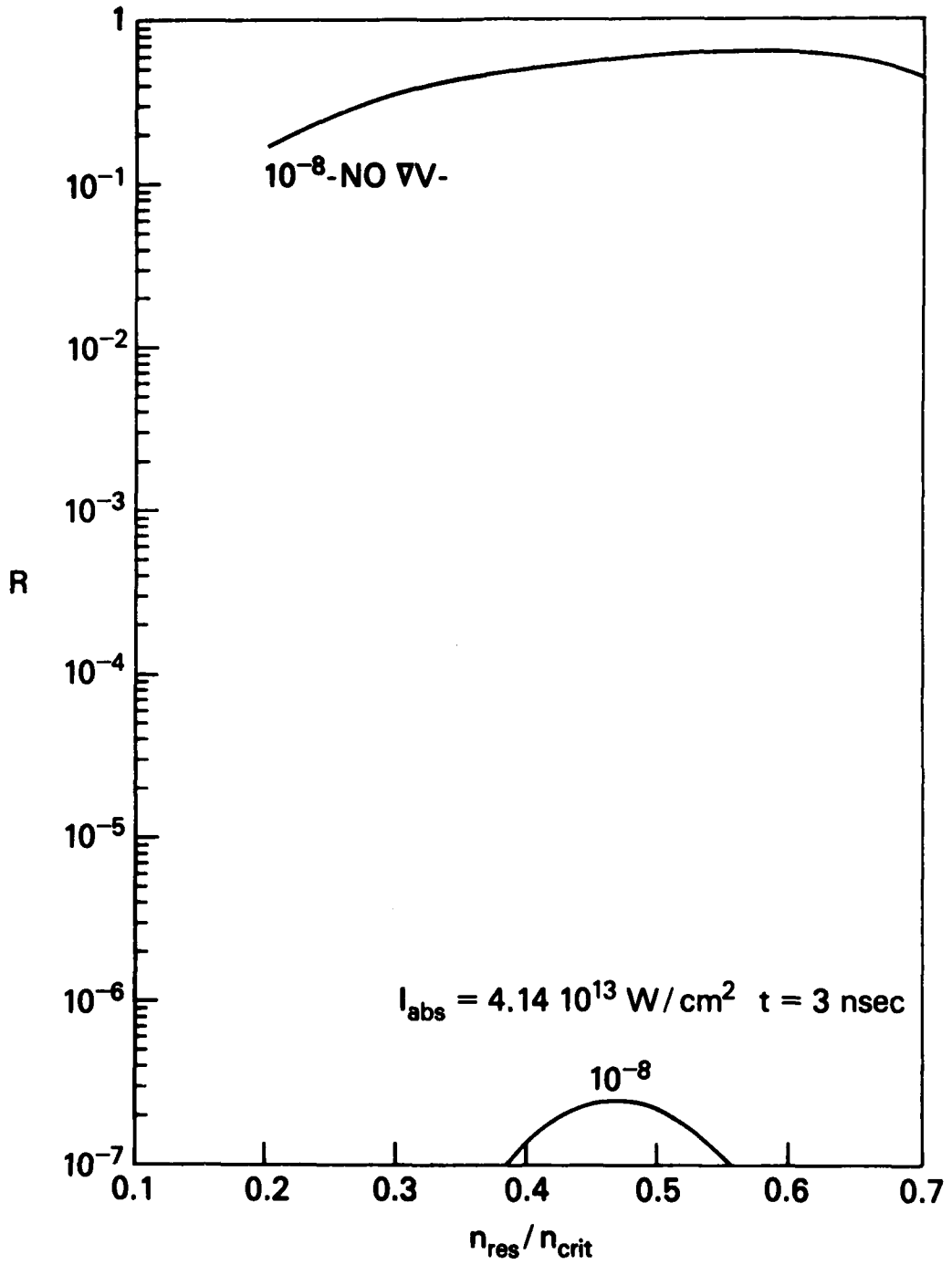

Fig. 3 Influence of velocity gradients on reflectivity as a function of resonant density for target of Fig. 1 and I_{abs} = 4.1 10 ^{13} W/cm^2.

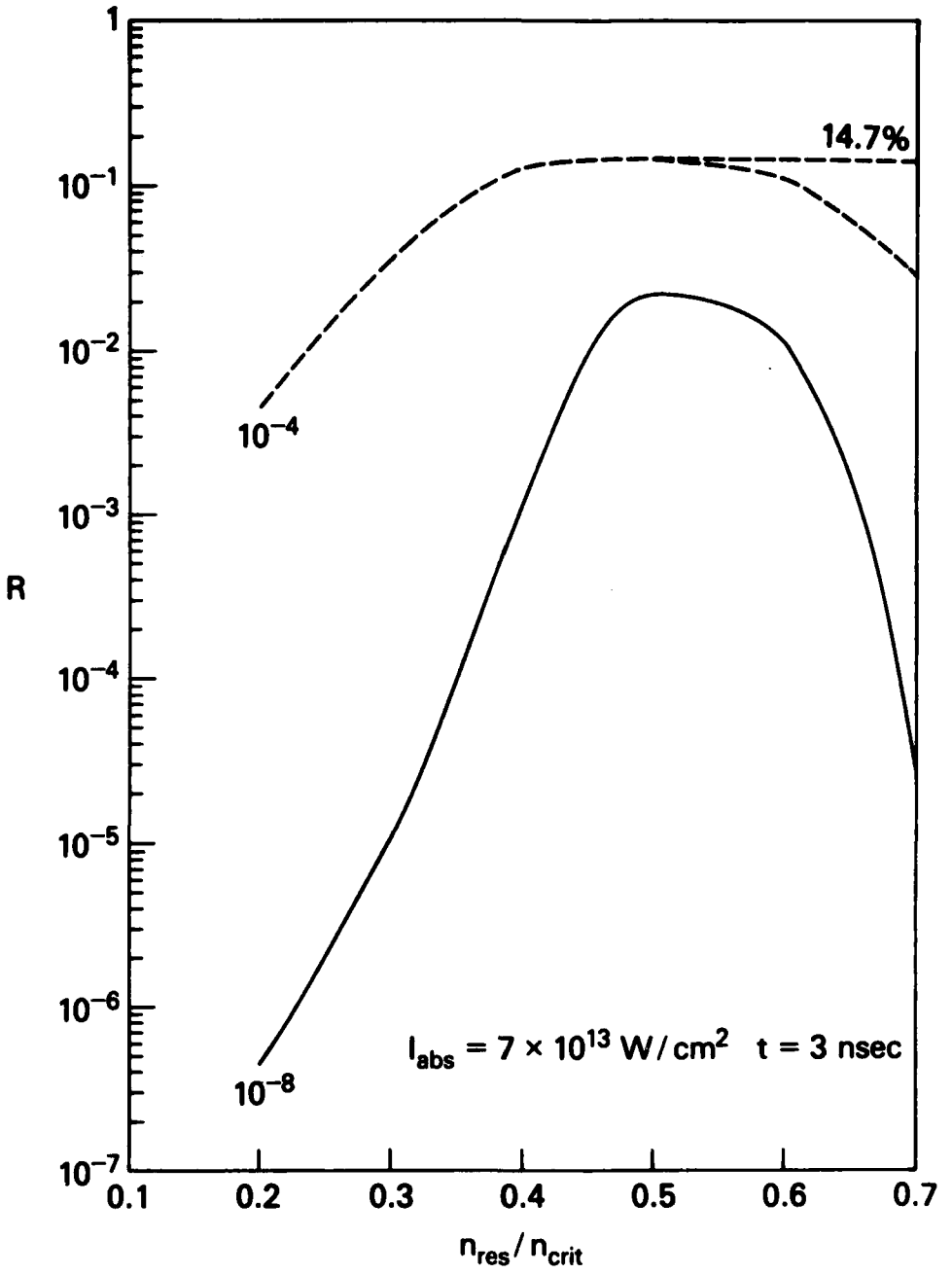

Fig. 4 Influence of thermal noise initial amplitude on reflectivity as a function of resonant density for target of Fig. 1 and $I_{abs} = 7.10^{13}$ W/cm^2. Note that for low values of reflectivity (less that 1% for upper curve), reflectivity varies linearly with thermal noise amplitude. For higher reflectivity, non-linear effects (pump depletion) reduce the difference between the two cases.

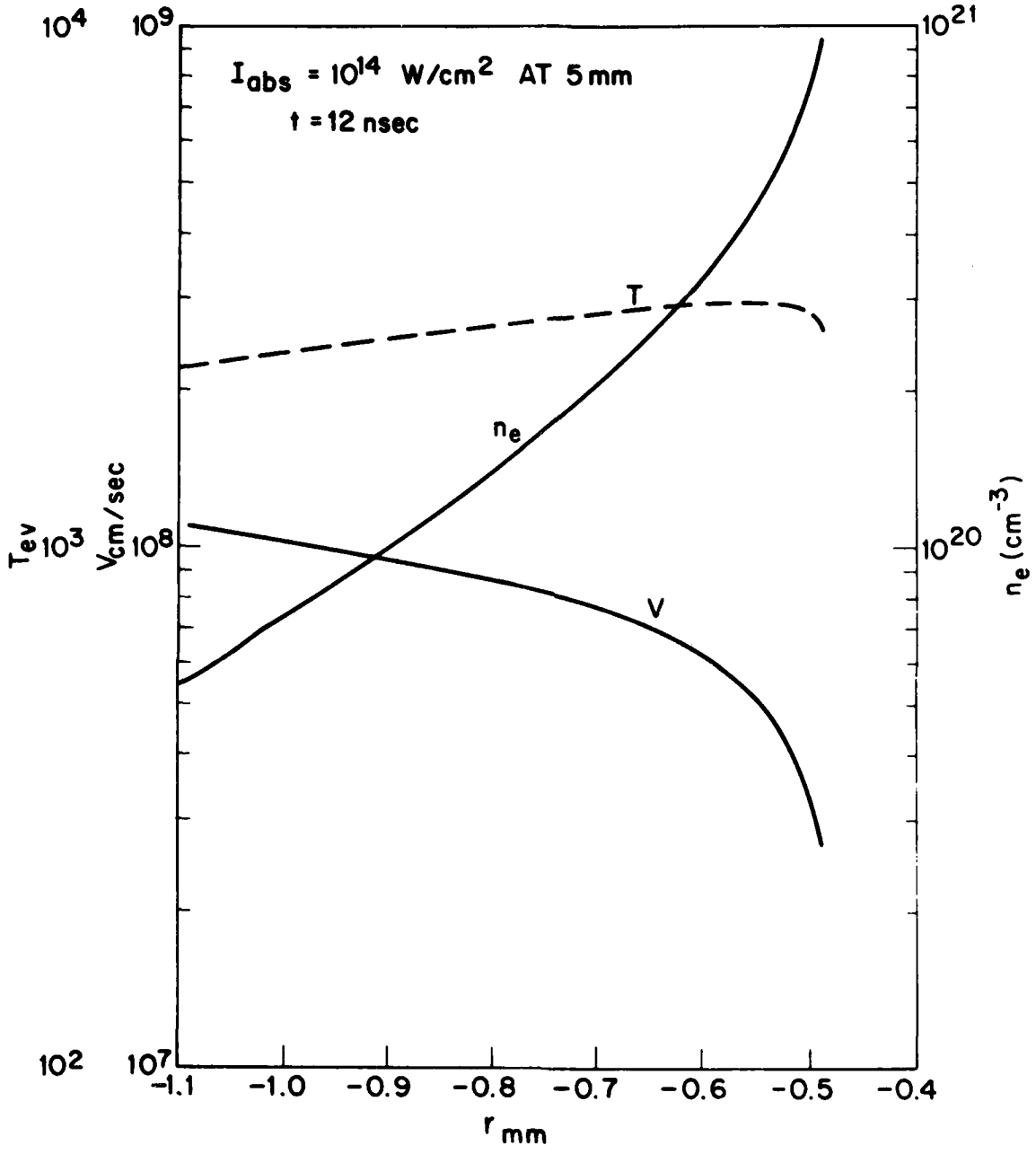

Fig. 5 Flow profiles for 10^{14} W/cm^2 absorbed, 1 μ laser light impinging on 5 mm radius spherical target at t = 12 nsec.

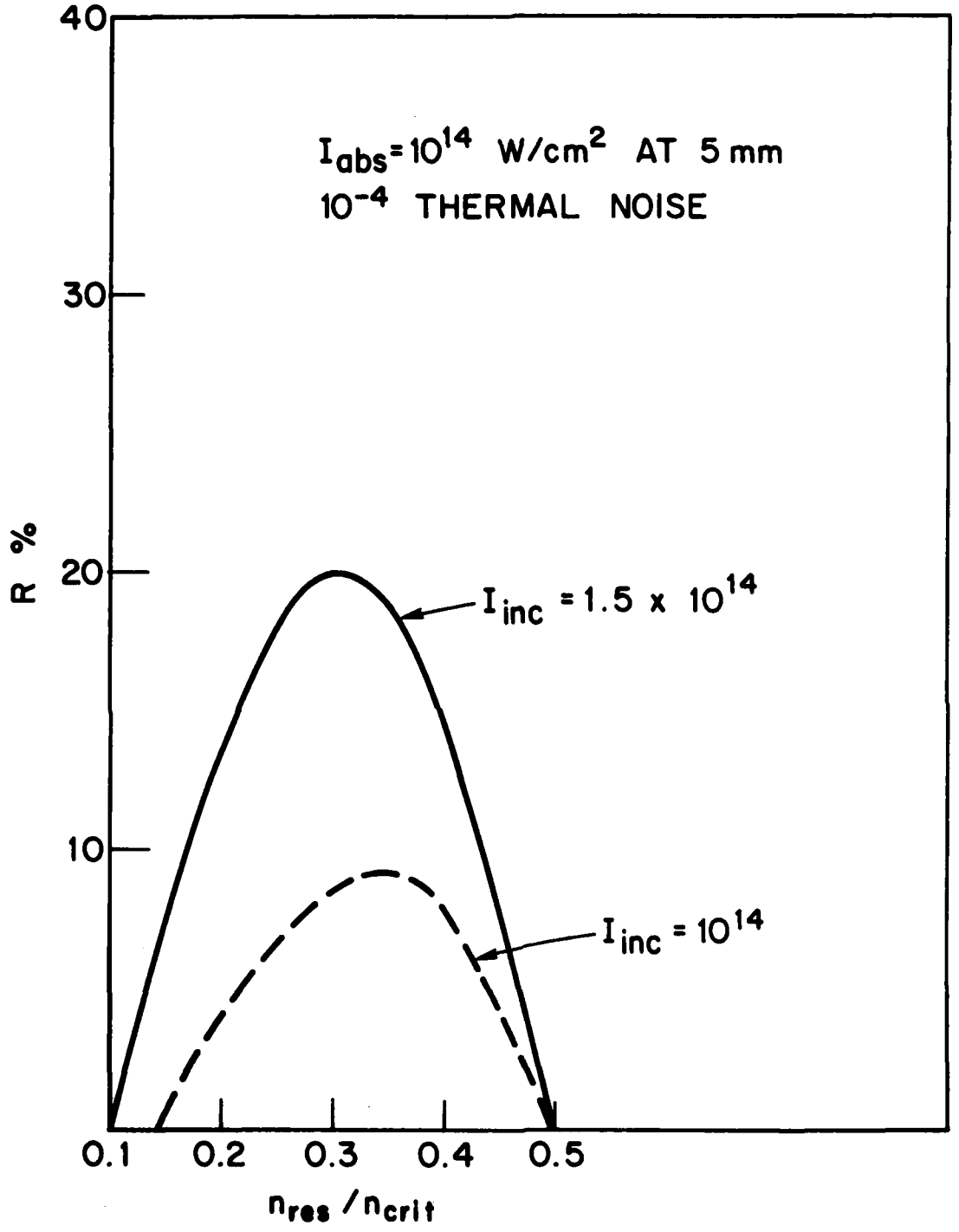

Fig. 6 Reflectivity for the case of Fig. 5 as a function of the resonant density of the reflected wave. Curves correspond to incident irradiance of 1.5 10^{14} W/cm^2 and 10^{14} W/cm^2.

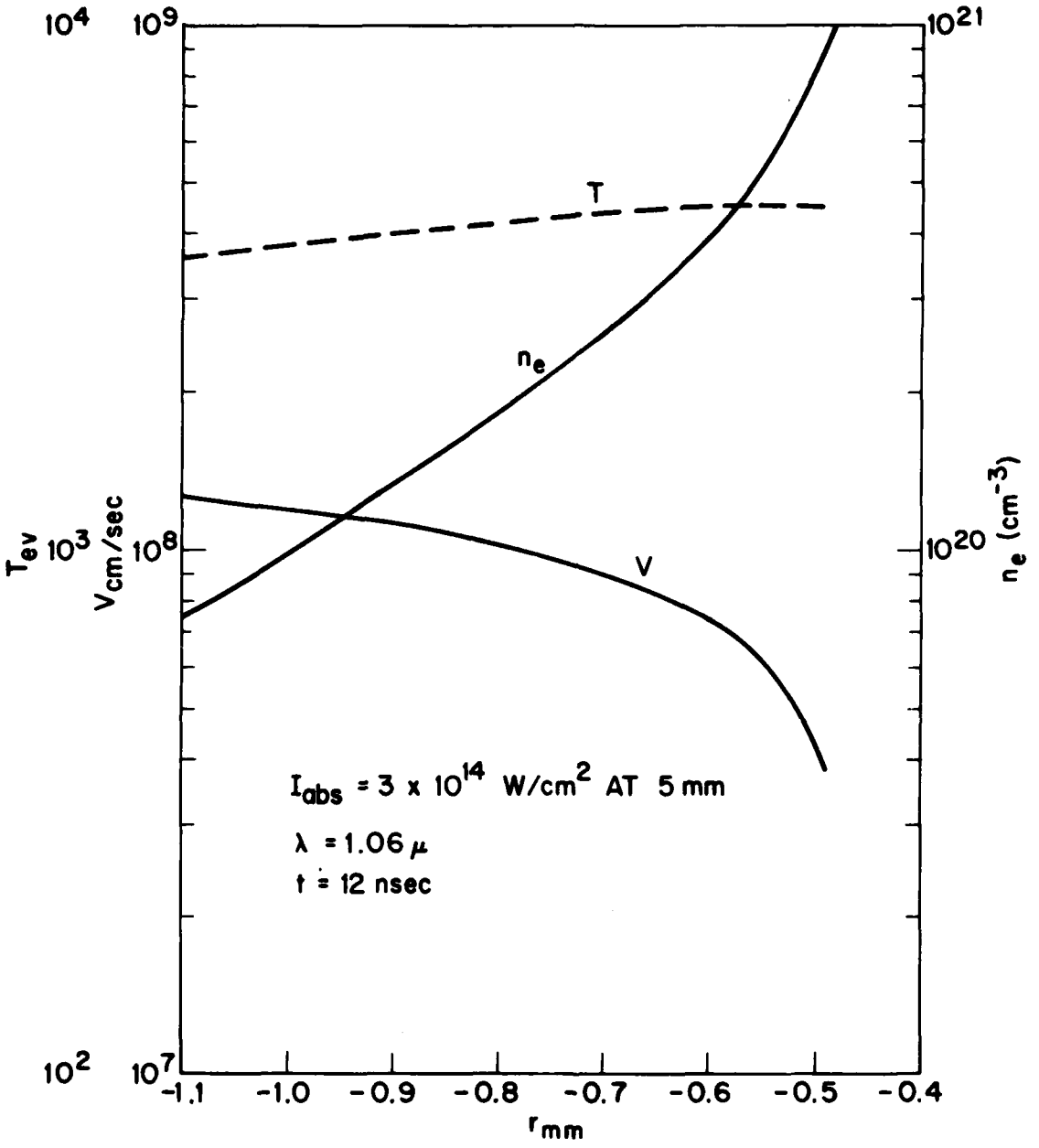

Fig. 7 Flow profiles for 3 x 10^{14} W/cm^2 absorbed, 1 μ laser light impinging on 5 mm radius spherical target at t = 12 nsec.

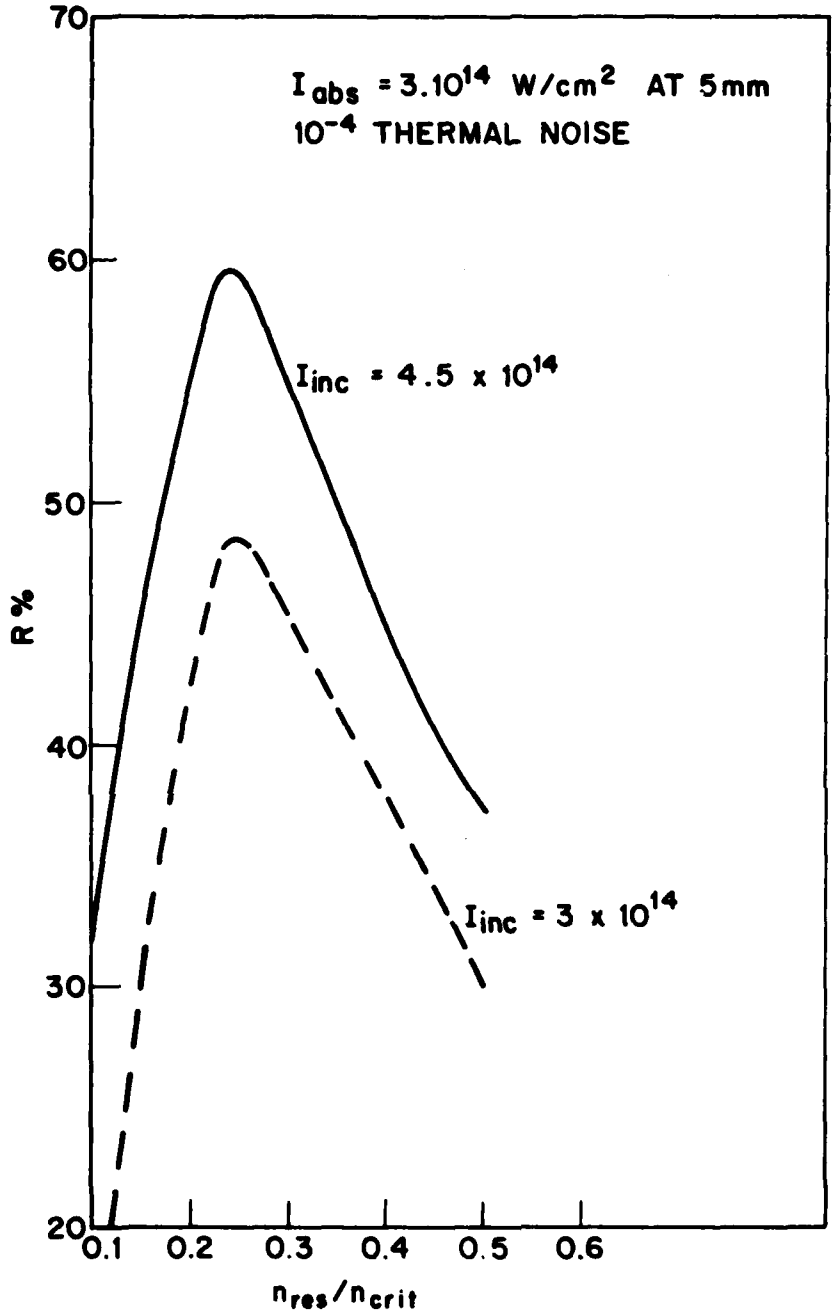

Fig. 8 Reflectivity for the case of Fig. 7, 1 μ laser light as a function of resonant density. Curves correspond to incident irradiance of 4.5 10^{14} W/cm^2 and 3 x 10^{14} W/cm^2.

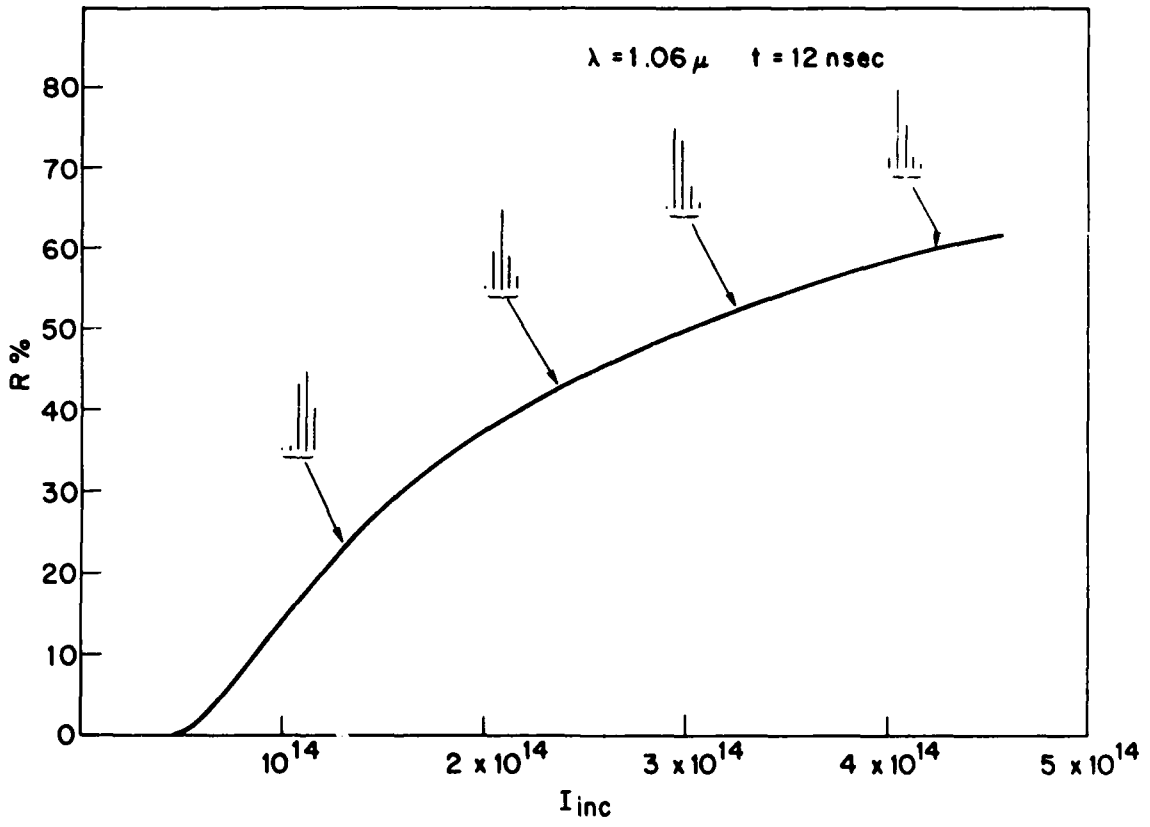

Fig. 9 Reflectivity as a function of incident irradiance for profiles and laser characteristics of Fig. 7. This calculation assumes five simultaneous resonant modes n_{res}/n_{crit} = 0.1 - 0.5. Note relative backscattered waves spectrum at 4 incident irradiances.

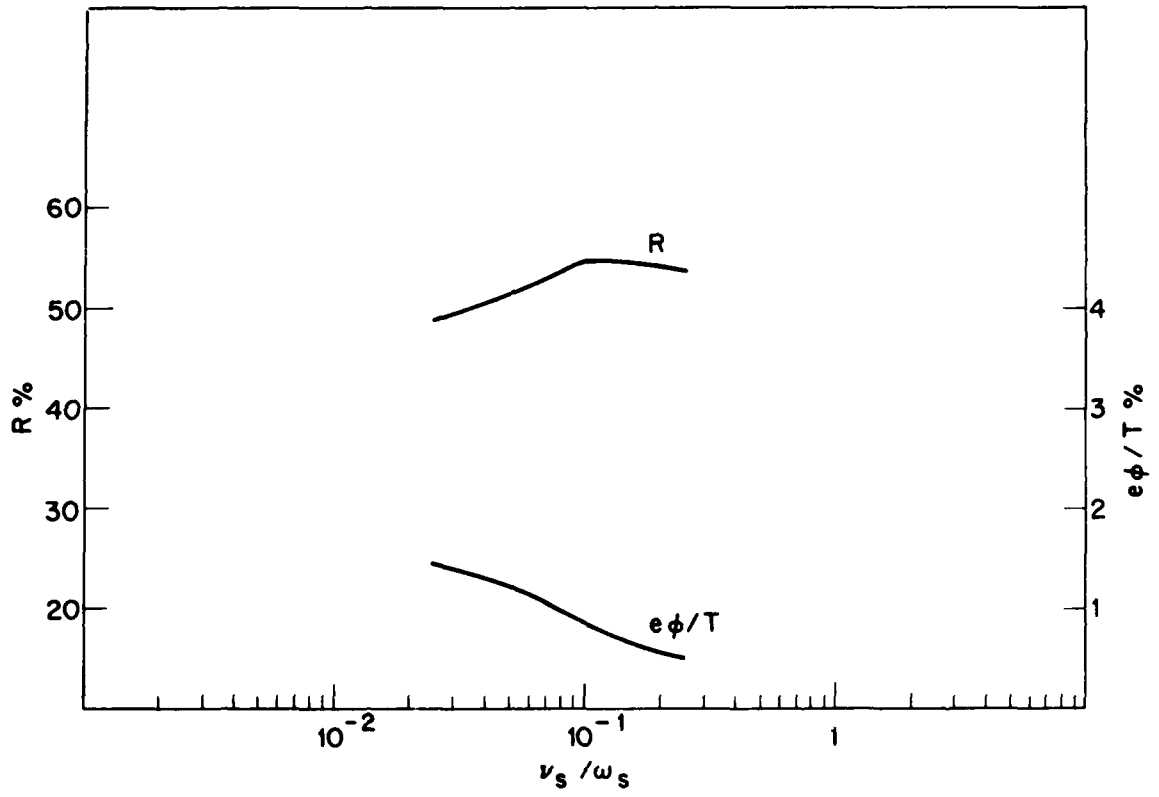

Fig. 10 Influence of dissipation rates on reflectivity and maximum value of $e\phi/T$. The calculation is the same as that in Fig. 8 (upper curve) for $n_{res}/n_{crit} = 0.3$.

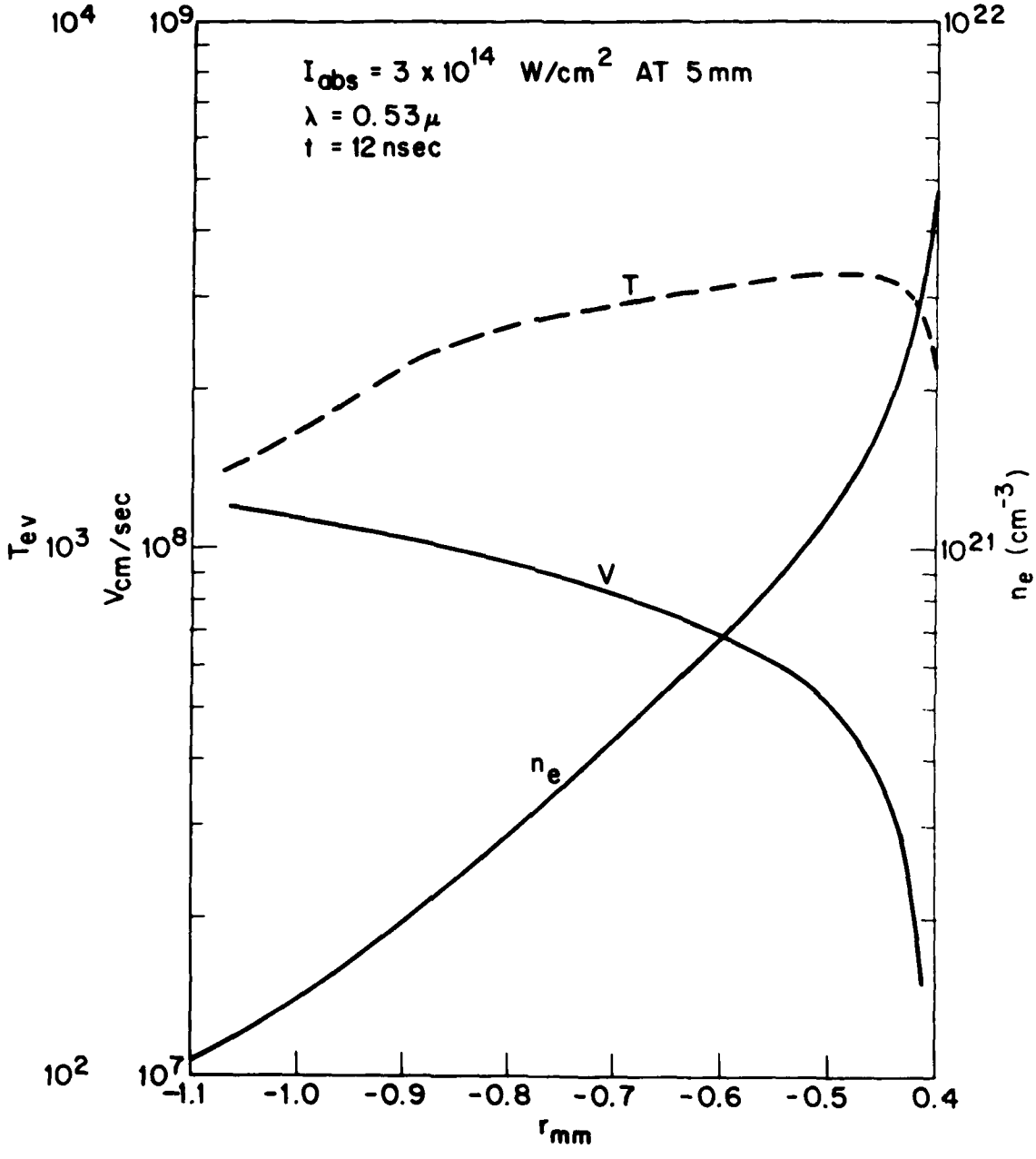

Fig. 11 Flow profiles for 3×10^{14} W/cm^2 absorbed, 0.53 μ laser light interacting with a 5 mm radius spherical target at t = 12 nsec.

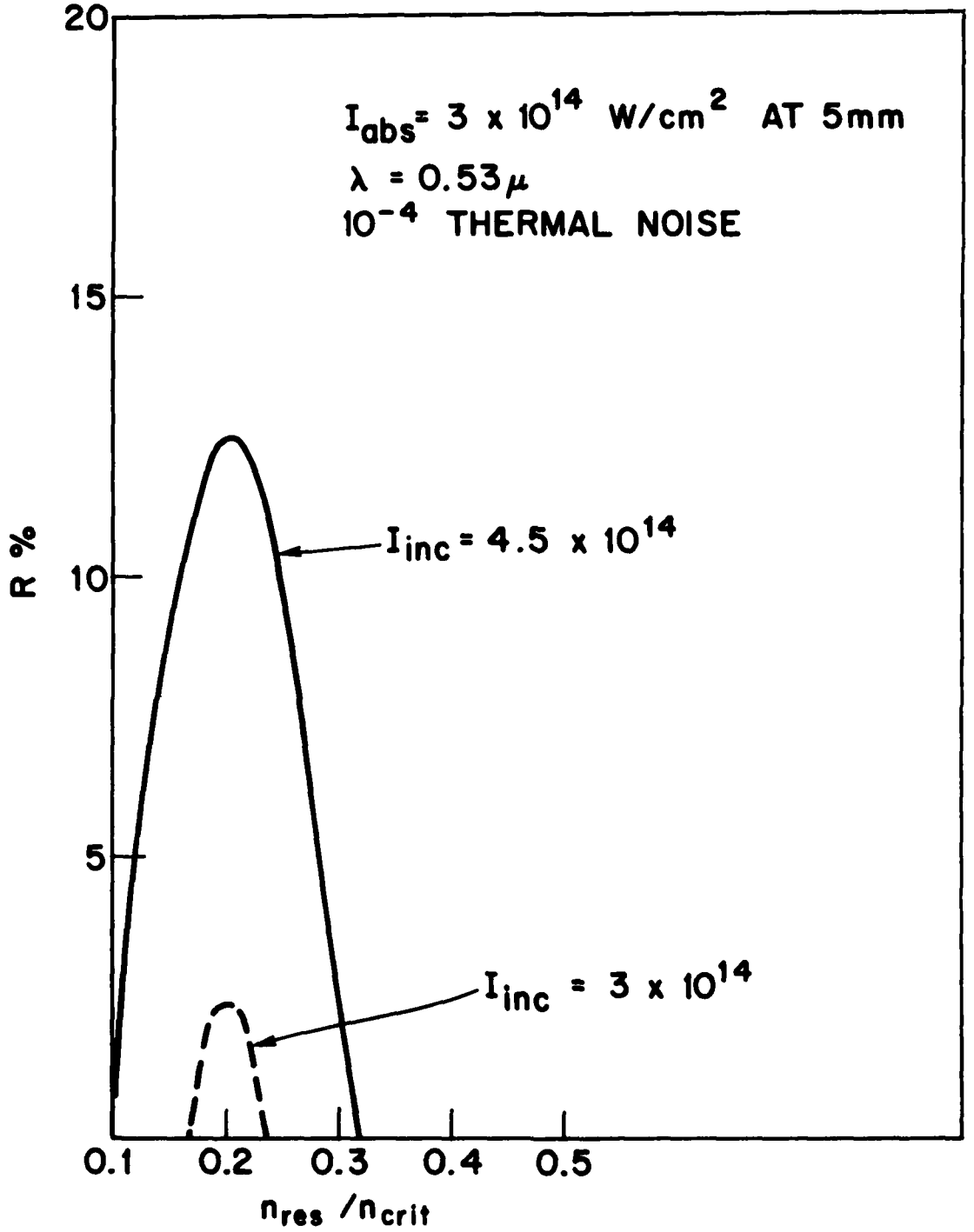

Fig. 12 Reflectivity for the case of Fig. 11, $\frac{1}{2}\mu$ laser light as a function of resonant density.

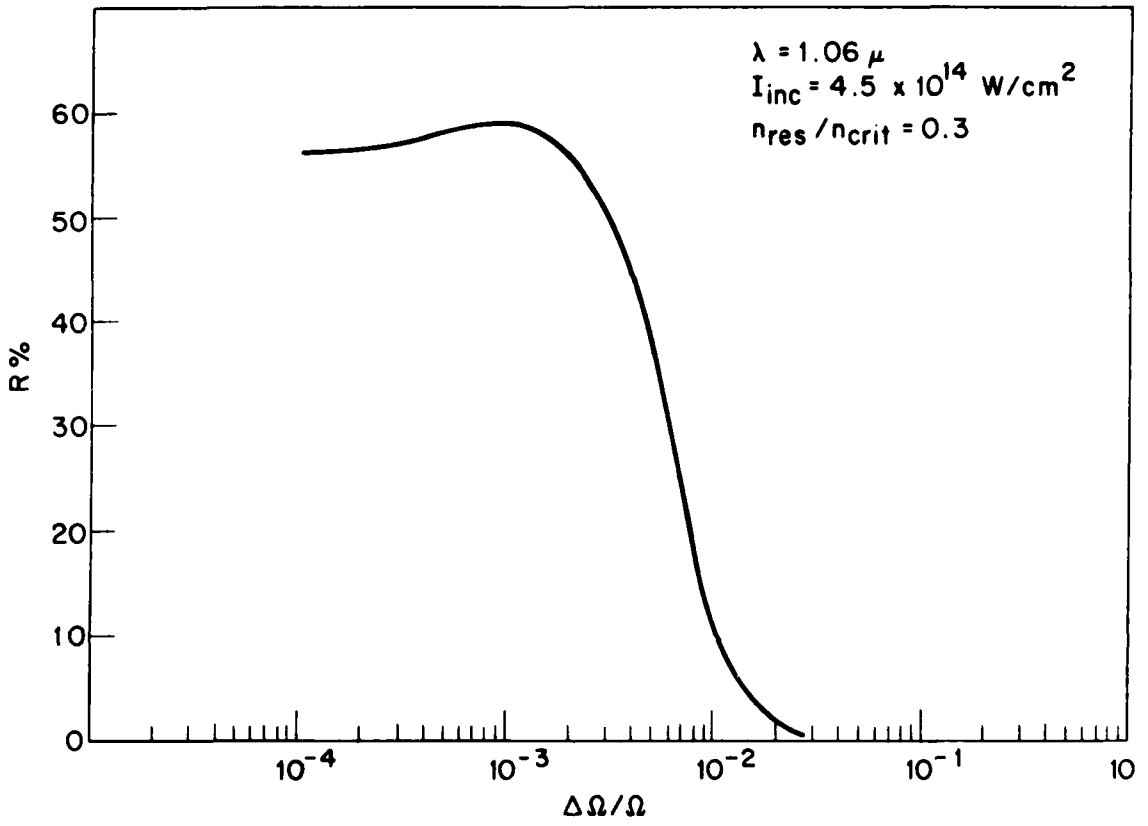

Fig. 13 Reflectivity for the case of Fig. 7, broadband 1 μ laser light as a function of frequency spread $\Delta\Omega/\Omega$ ($\Delta\Omega$ represent the 1/2 width) for resonant density n_{res}/n_{crit} = 0.3. Note the complete reduction of backscattering for $\Delta\Omega/\Omega = 2 \times 10^{-2}$.

References

1. B. H. Ripin, R. DeCoste, S. P. Obenschain, S. E. Bodner, E. A. McLean, F. C. Young, R. R. Whitlock, C. M. Armstrong, J. Grun, J. A. Stamper, S. H. Gold, D. J. Nagel, R. H. Lehmberg and J. M. McMahon, Phys. Fluids 23, 1012 (1980) and 24, 990 (1981).
2. B. H. Ripin, S. E. Bodner, P. G. Burkhalter, H. Griem, J. Grun, H. Hellfeld, M. J. Herbst, R. H. Lehmberg, C. K. Manka, E. A. McLean, S. P. Obenschain, J. A. Stamper, R. R. Whitlock and F. C. Young, 9th International Conference on Plasma Physics, Baltimore, Paper IAEA-CN-41/B-3 (1982), also NRL Memorandum Report 4916 (1982)
3. M. H. Key, R. G. Evans, P. T. Rumsby, C. L. S. Lewis, J. M. Ward and R. L. Cooke, Phys. Rev. Lett. 45, 1801 (1980).
4. S. P. Obenschain, R. R. Whitlock, E. A. McLean, B. H. Ripin, R. H. Price, D. Phillion, E. M. Campbell, M. D. Rosen, and J. M. Auerbach, Phys. Rev. Lett. 50, 44 (1983).
5. W. M. Manheimer and D. G. Colombant, Phys. Fluids, 24, 2319 (1981).
6. A. Ramani and C. E. Max, Phys. Fluids, to be published.
7. J. H. Gardner and S. E. Bodner, Phys. Rev. Lett. 47, 1137 (1981).
8. F. Amiranoff, R. Benattar, R. Fabbro, E. Fabre, C. Garban, C. Popovics, A. Poquerusse, R. Sigel, C. Stenz, J. Virmont and M. Weinfeld, in Plasma Physics and Controlled Nuclear Fusion Research (IAEA, Vienna, 1978), Vol. III p. 75.